

Published in final edited form as:

Bioorg Med Chem Lett. 2013 November 15; 23(22): . doi:10.1016/j.bmcl.2013.08.112.

Discovery of *N*-(benzo[1,2,3]triazol-1-yl)-*N*-(benzyl)acetamido)phenyl) carboxamides as severe acute respiratory syndrome coronavirus (SARS-CoV) 3CLpro inhibitors: identification of ML300 and non-covalent nanomolar inhibitors with an induced-fit binding

Mark Turlington^{a,b,c}, Aspen Chun^{a,b,c}, Sakshi Tomar^d, Aimee Egger^d, Valerie Grum-Tokars^e, Jon Jacobs^{a,b,c}, J. Scott Daniels^{a,b,c}, Eric Dawson^{a,b,c}, Adrian Saldanha^f, Peter Chase^f, Yahir M. Baez-Santos^d, Craig W. Lindsley^{a,b,c,g}, Peter Hodder^f, Andrew Mesecar^{d,*}, and Shaun R. Stauffer^{a,b,c,g,*}

^aDepartment of Pharmacology, Vanderbilt University Medical Center, Nashville, TN 37232, USA

^bVanderbilt Center for Neuroscience Drug Discovery, Vanderbilt University Medical Center, Nashville, TN 37232, USA

^cVanderbilt Specialized Chemistry Center for Probe Development (MLPCN), Nashville, TN 37232, USA

^dDepartment of Biological Sciences, Purdue University, West Lafayette, IN 47907, USA

^eDepartment of Molecular Pharmacology and Biological Chemistry, Northwestern University, Chicago, Illinois 60607, USA

^fScripps Research Institute Molecular Screening Center, Lead Identification Division, Translational Research Institute, Jupiter, FL 33458, USA

^gDepartment of Chemistry, Vanderbilt University, Nashville, TN 37232, USA

Abstract

Herein we report the discovery and SAR of a novel series of SARS-CoV 3CLpro inhibitors identified through the NIH Molecular Libraries Probe Production Centers Network (MLPCN). In addition to ML188, ML300 represents the second probe declared for 3CLpro from this collaborative effort. The X-ray structure of SARS-CoV 3CLpro bound with a ML300 analog highlights a unique induced-fit reorganization of the S₂-S₄ binding pockets leading to the first sub-micromolar non-covalent 3CLpro inhibitors retaining a single amide bond.

Keywords

3CLpro; severe acute respiratory syndrome; SARS; MERS; coronavirus

© 2013 Elsevier Ltd. All rights reserved.

*To whom correspondence should be addressed: shaun.stauffer@vanderbilt.edu.

Publisher's Disclaimer: This is a PDF file of an unedited manuscript that has been accepted for publication. As a service to our customers we are providing this early version of the manuscript. The manuscript will undergo copyediting, typesetting, and review of the resulting proof before it is published in its final citable form. Please note that during the production process errors may be discovered which could affect the content, and all legal disclaimers that apply to the journal pertain.

Coronaviruses (CoV) are enveloped, large plus-strand RNA viruses associated with mild to severe respiratory symptoms, including the common cold and the Severe Acquired Respiratory Syndrome (SARS)-CoV.¹⁻³ Identified as the etiological agent responsible for the global pandemic in 2003, SARS presents an atypical pneumonia that during the first major outbreak led to progressive respiratory failure in over 8,000 individuals and about 800 deaths by July of that year.⁴ With the cooperation of leading nations, a rigorous public healthcare campaign was fortunately successful in controlling this outbreak. However, a reemergence of the SARS-CoV is considered a potential pandemic risk and new strains of human coronavirus continue to be identified. Since 2003, two additional human coronaviruses, NL63 and HKU1, have been identified in patients and the viruses have been characterized and found to be significantly less lethal than SARS-CoV.⁵⁻⁷ Most recently in 2012, a new SARS-like virus, designated the Middle East respiratory syndrome coronavirus (MERS-CoV), has been identified in 77 patients so far, 40 of whom died.⁸ There is now evidence for person-to-person transmission of MERS-CoV.⁹ Now, nearly a decade later, the possibility of another SARS-like pandemic appears even more palpable based upon the lethality and properties of the newly identified MEV-HCoV strain. Effective vaccines and small molecule antiviral agents to prevent or treat SARS-like infections still do not exist, thus tailored antiviral therapies are urgently needed in order to treat potential future outbreaks of SARs and related human coronaviruses.

The SARS and MERS coronaviruses encode two proteases, a papain-like protease (PLpro) and a 3 chymotrypsin-like protease (3CLpro), in their genome that are essential for viral replication. The viral polyprotein is cleaved at 3 unique sites by PLpro and 11 unique sites by 3CLpro. Initial reports of 3CLpro inhibitors in the literature focused on peptidomimetics, often four to five residues in length, bearing a reactive “warhead” group, such as an aldehyde, halo-methyl ketone, or Michael acceptor at the terminus with several demonstrating a covalent interaction with the active site Cys-145 residue.¹⁰⁻¹⁶ Until recently, the majority of efforts to develop non-peptidic 3CLpro inhibitors also relied on “warhead” based design strategies (Fig. 1, **1-5**)¹⁷⁻²¹ and a number of these non-peptidic inhibitors achieved sub-micromolar activity. In the case of pyridyl ester **4**,²⁰ this potent nanomolar mechanism-based enzyme inactivator led to cell based inhibition below 10 μM in SARS-CoV infected Vero E6 cells. Recently, we reported *N*-(*tert*-butyl)-2-(*N*-arylamido)-2-(pyridin-3-yl) acetamide **6** (Fig. 1, ML188) and its X-ray complex with 3CLpro (PDB: 3V3M) as a rare example of a non-covalent SARS-CoV 3CLpro inhibitor of moderate molecular weight with good enzyme and antiviral inhibitory activity.²² Herein, we describe the continuation of efforts to develop potent, non-covalent SARS-3CLpro inhibitors based upon a second chemical class of triazoles from our MLPCN screening campaign (**7**, Fig. 2) and progression of this lead series to a second generation probe ML300 (**8**, Fig. 8) and beyond to arrive at sub-100 nM inhibitors. We propose from crystallography data that ML300 and related triazoles in this series inhibit 3CLpro via a novel mechanism of action and provide a new direction for additional non-covalent inhibitor design and refinement.

Using a designed expression construct which produces the post-proteolytic and authentic 3CLpro dimer, a screen against the NIH molecular libraries sample collection (~293K compounds) at the Scripps Research Institute Molecular Screening Center (SRIMSC) was undertaken. In addition to the diamide acetamide series represented by ML188 (**6**, Fig. 1),²² a related diamide series, represented by SID 24808289 (**7**, Fig. 2), was identified demonstrating a 3CLpro IC₅₀ of 6.2 μM and good selectivity vs. PLpro (IC₅₀ > 60 μM) which is used as a control for cysteine-protease activity. Fortunately, quite early in the chemistry campaign an X-ray crystal structure of diamide **7** bound to 3CLpro was determined to 1.85 Å resolution. A solvent accessible surface depiction of **7** in the 3CLpro active site along with a wall-eye stereo view with key contact residues and hydrogen bonding contacts in depicted in Figure 3 (Fig. 3). Interestingly, in contrast to the ML188-3CLpro

crystal structure in which ML188 accommodates substrate sub-pockets in the enzyme active-site traditionally occupied by peptidomimetics, diamide **7** engenders an induced-fit complex resulting in a new surface dictated largely by a rearrangement of the Gln-189 and Met-49 residue side-chains.²³ This induced fit accommodates the *syn* *N*-methyl pyrrole and anilido acetamide moieties of the inhibitor within subpockets that can be characterized as S₂-S₄ and S₂-S₁, subpockets, respectively.

Figure 2 schematically illustrates the inhibitor-active site interactions oriented in a manner similar as depicted in Figure 3. In addition to the P₂-P₄ and P₂-P₁, groups the inhibitor partially occupies the S₃ subpocket with a terminating 2-methylbutylamide. Key hydrogen bonding interactions can be found near the catalytic site with His-163 and the benzotriazole *N*-(3) engaged in a key interaction, with an interatomic distance of 2.9 Å. In addition a backbone Glu-166 NH interaction is evident with the central acetamide oxygen (N-O distance 2.8 Å).

Flexibility of the diamide scaffold (RotBon ~ **7**) coupled with the observed induced-fit within the active site of 3CLpro presents an added challenge with respect to *in silico* inhibitor approaches. Thus, our structure-activity-relationship (SAR) studies focused initially on three key areas within the diamide scaffold: 1) benzotriazole replacements with alternative hydrogen bond acceptor functionality to interact with His-163, 2) acetamide modifications within the P₂-P₁, region, and 3) minimum pharmacophore deletion studies of the P₃ 2-methylbutylamide. The P₂-P₄ group was held constant for this investigation and based upon HTS and reconfirmation results (data not shown) the *N*-methyl pyrrole was replaced with an equipotent 3-thienyl moiety.

In parallel with efforts to obtain the 3CLpro-**7** crystal structure, synthesis of first generation analogs to survey diversity of the benzotriazole unit were initiated using a modified version of our 4CC-Ugi strategy (Scheme 1) to allow for late stage azole introduction. Thus, Ugi reaction using *t*-butyl isocyanide, chloroacetic acid, thiophene-3-carbaldehyde, and *N*-(4-aminophenyl)acetamide proceeded smoothly to give chloride **8**, which could be isolated in good yield after chromatography. Displacement of chloride **8** with azole NH heterocycles provided **9a–c**. Alternatively, displacement of **8** with sodium azide and subsequent Huisgen cycloaddition reaction with an appropriate acetylene furnished 1,2,3-triazoles **10a–c** in good overall yield.

Synthesis of P₂-P₁, amide analogs within the elaborated diamide were similarly prepared in an Ugi reaction using Boc-protected 4-(amino) aniline (Scheme 2) as the amine component. Deprotection of **11** using trifluoroacetic gave aniline **12** which was reacted with a variety of carboxylic acid derivatives under HATU coupling conditions or reacted with an acid chloride or sulfonyl chloride in the presence of TEA to give final examples **13a–l**.

Synthesis of P₃ truncated analogs began with reductive amination using thiophene-3-carbaldehyde with either 4-bromoaniline or Boc-protected 4-(amino) aniline to give intermediates **14a–b** in good yield. Amide coupling with HATU using benzotriazol-1-yl-acetic acid installed the requisite P₁ groups to afford **15a–b**. Initial efforts focused on preparing the identical amide library prepared in the elaborated series **13**. This was readily accomplished as before; Boc-deprotection of **15a** followed by amide coupling or acylation/sulfonylation, gave **16a–k**. Subsequent synthesis of a series of biaryls as amide replacements commenced using a Suzuki cross-coupling with **15b** and a variety of boronic acids to afford target molecules **17a–e**.

SAR for 1,3-azole P₁ replacements (**9a–c**, Fig. 4) indicated a strict requirement for the 1,2,3-triazole unit; benzimidazoles **9a–b** and 2-methyl-1-imidozyl derivative **9c** were uniformly

inactive. Since the *N*-(3) nitrogen of **7** appeared to be involved in a hydrogen bond with His-163, it was somewhat surprising that **9a** was not tolerated since the imidazole has the potential to maintain a *N*-(3)-His-163 hydrogen bond interaction. However, within the 3CLpro-**7** structure the catalytic Cys-145 residue is located within 3.3 Å of the *N*-(2) nitrogen, indicating potential for a weak hydrogen bond and/or dipole-dipole stabilization interaction. This potential interaction may perhaps be responsible for the 1,2,3-triazole preference. Interestingly, 4-phenyl 1,2,3-triazole **10c** was tolerated with an IC₅₀ of 11 μM, suggesting additional avenues for optimization. Accommodation of the phenyl moiety of **10c** within the active site S₁ subpocket is not entirely clear at this time. Based on the 3CLpro-**7** structure, Glu-166, Phe-140, and Glu-166 are predicted to be within close proximity. Unsubstituted triazole **10a** and trimethyl silyl triazole **10b** were inactive, demonstrating the importance of maintaining a proper aromatic ring in this subpocket.

Amide library **13a–l** (Fig. 5) within the elaborated diamide series displayed a range of potency from moderate micromolar activity (**13a**, **13b–d**, **13f–g**) comparable to the HTS hit **7**, to weakly active or inactive. Cyclic and acyclic acetamide congeners related to HTS lead **7** showed consistent activities below 10 μM with branched *i*-propyl derivative **13d** and cyclobutyl amide **13g** having the greatest activity below 5 μM. Modification to sulfonamide **13b** resulted in a three-fold loss in inhibition relative to acetamide **13a**. The smaller cyclopropyl (**13f**) or larger cyclohexyl (**13h**) cyclic amide generally resulted in loss of inhibition. Incorporating a sterically hindered *t*-butyl amide **13e** also led to a modest three-fold loss in activity. Lastly, aromatic and heteroaromatic amides (**13i–k**) in addition to *iso*-butyl carbamate **13l** were weak or inactive as 3CLpro inhibitors. Collectively, these data appear to be consistent with the 3CLpro-**7** structure whereby a short helix-loop-helix motif (Val-42-Ile-43-Cys-44-Thr-45-Ala-46) and a proximal β-turn element (Thr-24-Thr-25) define the edge of this pocket with minimal volume for larger groups beyond acetamide **7**.

With limited success from the above S₁ and S₂-S₁, studies we turned to P₃ truncation to potentially identify a minimum pharmacophore to reduce overall MW and improve ligand efficiency (LE).²⁴ Examination of the P₃ group within the 7-3CLpro structure suggested this group was unfavorably solvent exposed relative to the *t*-butylamide-S₃ interaction found within the ML188-3CLpro structure.²² Initial efforts led to **16a–k** (Table 1). Gratifyingly truncated amides proved to have comparable activity versus the elaborated diamide counterparts (Fig. 5 see **13c–d**, **13f–g**, vs Table 1 see **16a–c**, **16e–f**). Interestingly, truncated series **16** appeared to better tolerate larger substituents, perhaps suggesting additional changes in the shape of the active site within this subpocket. For example cyclohexyl amide **16g** was found to be a weak inhibitor and similarly carbamate **16i** had moderate inhibitory activity of 10.3 μM while its related counterpart **13l** (Fig. 5) was inactive.

At this stage in the project with efforts focused on P₃ truncated analogs bearing a putative S₂-S₁ interaction, we elected **16e** for further characterization and probe declaration (ML300, Fig. 6). Relative to probe ML188 (**6**) and the equipotent diamide **13d**, ML300 proved to offer improvements in several areas (Fig. 6). SARS 3CLpro inhibitor ML300 is ~100 amu lower MW (MW=431) relative to **13d** with moderate ligand efficiency (LE). Deletion of the lipophilic P₃ group reduces cLogP an order of magnitude (cLogP=3.2) and thus greatly improves ligand-efficiency-dependent lipophilicity (LELP) versus ML188 and **13d**. Probe molecules ML188 and ML300 were evaluated in an in-house²⁵ *in vitro* DMPK panel including plasma protein binding, P450 enzyme inhibition, and intrinsic clearance using liver microsomes (Fig. 6). Both ML188 and ML300 possess good free fraction with ML300 being superior (1.5 and 4.0-fold improved human and rat fraction unbound, respectively); however, intrinsic clearance (CL_{HEP} normalized to liver blood flow, Q_h = 21 mL/min/kg, Q_r = 70 mL/min/kg) indicates ML188 and both ML300 are predicted to be highly cleared. ML188 and ML300 possess modest P450 enzyme inhibition, with ML300

maintaining 5–10 μM activity across four major CYP enzymes (Fig. 6). Probe ML300 was found to be highly selective in a Eurofins lead-profiling screen²⁶ with only modest activity for melatonin MT₁ receptor in a radioligand binding assay.

Based on the absence of key hydrogen bonding interactions of the P₂-P₁, amide of **7** with the 3CLpro active site, in addition to the poor metabolic instability and CYP profile of ML300, we opted to explore more diverse amide replacements as a means to improve metabolic stability, P450 activity, and 3CLpro inhibitory potency. Initial efforts identified representative *N*-methyl (**16j**) and *N*-benzyl (**16k**) anilines with potency comparable to probe ML300 (**16e**). The lack of activity for benzamide **16h** versus the reduced benzylamine **16k** is striking and indicates the enhanced flexibility of the *N*-benzyl group is permitting a productive interaction to occur where previously aromatic amides were not tolerated (see Fig. 5, **13i–j**). A subsequent survey of biaryls was explored (Table 1 **17a–e**) and on the basis of the 3CLpro-**7** X-ray we targeted 3-pyridyl (**17b–c**) and 4-pyrimidyl (**17e**) heterocycles as means to potentially engage a side-chain interaction from the hydroxyl groups of Thr-24 or Thr-25. These modifications afforded inhibitors with micromolar activity and in the case of 2-methoxypyridyl **17c** submicromolar activity (IC₅₀ = 700 nM). Unexpectedly the parent simple phenyl biaryl **17a** proved to have a major impact on activity with a ~7–10-fold increase relative to **17b–c**. 3CLpro inhibitor **17a** represented the first sub-100 nM inhibitor for the series and to our knowledge one of the most potent non-warhead based SARS 3CLpro inhibitors to date. At this time inhibitor **17a** is relatively unoptimized and thus current efforts are focused on targeted biaryl congeners to understand DMPK, cellular activity, as well as potential broad spectrum activity against other coronavirus strains including MERS-CoV.

In summary, we have described the identification and binding orientation and interactions for a second class of diamide SARS 3CLpro inhibitors, culminating in probe ML300 and subsequently improved inhibitors such as **17a**, which possess LE > 0.3 and an LELP approaching 10. The X-ray crystal structure of HTS hit **7** bound to 3CLpro²⁷ was instrumental in guiding optimization and the induced-fit of this inhibitor 3CLpro complex illustrates the challenges of divergent SAR and the limitations of virtual based screens. The four component Ugi reaction was utilized once more to rapidly generate SAR for the putative P₂-P₁, and P₁ subgroups. Importantly, P₃ truncation was possible for this triazole series of 3CLpro inhibitors, allowing for significant MW reduction without diminishing potency. Collaborative efforts in these laboratories continue towards the identification active inhibitors within the truncated biaryl class. Integrated efforts with DMPK assessment continue in order to improve intrinsic clearance and diminish P450 activity, which are issues to be addressed within the series prior to in vivo proof-of-mechanism studies. ML300 is an MLPCN probe and is freely available upon request.

Acknowledgments

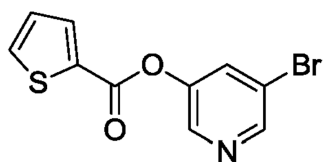
This work was supported in part by MLPCN (1U54 MH084659 and MH084512) and NIAID to ADM (AI060915, AI026603 and AI085089). The authors thank the synchrotron beamline (LS-CAT) personnel at the Advanced Photon Source at Argonne National Lab. Use of the Advanced Photon Source, an Office of Science User Facility operated for the U.S. Department of Energy (DOE) Office of Science by Argonne National Laboratory, was supported by the U.S. DOE under Contract No. DE-AC02-06CH11357. Use of the LS-CAT Sector 21 was supported by the Michigan Economic Development Corporation and the Michigan Technology Tri-Corridor (Grant 085P1000817).

References and Notes

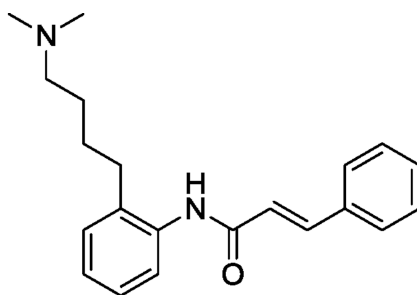
1. McIntosh K, Dees JH, Becker WB, Kapikian AZ, Chanock RM. Proc Natl Acad Sci U S A. 1967; 57:933. [PubMed: 5231356]

2. Myint, SH. Human coronavirus infections. Siddell, SG., editor. Plenum Press; 1995. p. 389
3. Ksiazek TG, Erdman D, Goldsmith CS, Zaki SR, Peret T, Emery S, Tong S, Urbani C, Comer JA, Lim W, Rollin PE, Dowell SF, Ling AE, Humphrey CD, Shieh WJ, Guarner J, Paddock CD, Rota P, Fields B, DeRisi J, Yang JY, Cox N, Hughes JM, LeDuc JW, Bellini WJ, Anderson LJ. N Engl J Med. 2003; 348:1953. [PubMed: 12690092]
4. Ziebuhr J. Curr Opin Microbiol. 2004; 7:412. [PubMed: 15358261]
5. Pyrc K, Berkhout B, van der Hoek L. J Virol. 2007; 81:3051. [PubMed: 17079323]
6. Fielding BC. Future Microbiol. 2011; 6:153. [PubMed: 21366416]
7. Cui L-J, Zhang C, Zhang T, Lu R-J, Xie Z-D, Zhang L-L, Liu C-Y, Zhou W-M, Ruan L, Ma X-J, Tan W-J. Advances in Virology. 2011:6. pages.
8. Centers for Disease Control and Prevention: <http://www.cdc.gov/coronavirus/mers/index.html>
9. a) Zaki AM, van Boheemen S, Bestebroer TM, Osterhaus AD, Fouchier RA. N Engl J Med. 2012; 367:1814. [PubMed: 23075143] b) Debing Y, Jochmans D, Neyts J. Current opinion in virology. 2013; 3:217. [PubMed: 23562753]
10. Ghosh AK, Xi D, Johnson ME, Baker SC, Mesecar AD. Ann. Rep. Med. Chem. 2006; Vol. 41:183.
11. Jain RP, Pettersson HI, Zhang J, Aull KD, Fortin PD, Huitema C, Eltis LD, Parrish JC, James MN, Wishart DS, Vederas JC. J Med Chem. 2004; 47:6113. [PubMed: 15566280]
12. Ghosh AK, Xi K, Ratia K, Santarsiero BD, Fu W, Harcourt BH, Rota PA, Baker SC, Johnson ME, Mesecar AD. J. Med. Chem. 2005; 48:6767. [PubMed: 16250632]
13. Yang S, Chen SJ, Hsu MF, Wu JD, Tseng CT, Liu YF, Chen HC, Kuo CW, Wu CS, Chang LW, Chen WC, Liao SY, Chang TY, Hung HH, Shr HL, Liu CY, Huang YA, Chang LY, Hsu JC, Peters CJ, Wang AH, Hsu MC. J Med Chem. 2006; 49:4971. [PubMed: 16884309]
14. Zhang J, Pettersson HI, Huitema C, Niu C, Yin J, James MNG, Eltis LD, Vederas JC. J. Med. Chem. 2007; 50:1850. [PubMed: 17381079]
15. Xue X, Yu H, Yang H, Xue F, Wu Z, Shen W, Li J, Zhou Z, Ding Y, Zhao Q, Zhang XC, Liao M, Bartlam M, Rao Z. J Virol. 2008; 82:2515. [PubMed: 18094151]
16. Akaji K, Konno H, Mitsui H, Teruya K, Shimamoto Y, Hattori Y, Ozaki T, Kusunoki M, Sanjoh A. J Med Chem. 2011; 54:7962. [PubMed: 22014094]
17. Blanchard JE, Elowe NH, Huitema C, Fortin PD, Cechetto JD, Eltis LD, Brown ED. Chem Biol. 2004; 11:1445. [PubMed: 15489171]
18. Chen WQ, Lu CY, Wong TW, Ling WH, Lin ZN, Hao YT, Liu Q, Fang JQ, He Y, Luo FT, Jing J, Ling L, Ma X, Liu YM, Chen GH, Huang J, Jiang YS, Jiang WQ, Zou HQ, Yan GM. Emerg Infect Dis. 2005; 11:89. [PubMed: 15705328]
19. Wu CY, King KY, Kuo CJ, Fang JM, Wu YT, Ho MY, Liao CL, Shie JJ, Liang PH, Wong CH. Chem Biol. 2006; 13:261. [PubMed: 16638531]
20. Ghosh AK, Gong G, Grum-Tokars V, Mulhearn DC, Baker SC, Coughlin M, Prabhakar BS, Sleeman K, Johnson ME, Mesecar AD. Bioorg Med Chem Lett. 2008; 18:5684. [PubMed: 18796354]
21. Zhang J, Huitema C, Niu C, Yin J, James MNG, Eltis LD, Vederas JC. Bioorg. Chem. 2008; 36:229. [PubMed: 18295820]
22. Jacobs J, Grum-Tokars V, Zhou Y, Turlington M, Saldanha SA, Chase P, Egger A, Dawson ES, Baez-Santos YM, Tomar S, Mielech AM, Baker SC, Lindsley CW, Hodder P, Mesecar A, Stauffer SR. J Med Chem. 2013; 56:534. [PubMed: 23231439]
23. For an example of 'induced-fit' and discussion on active-site flexibility in the context of inhibitor bound versus unbound SARS 3CLpro using an aza-peptide epoxide see: Lee TW, Cherney MM, Liu J, James KE, Powers JC, Eltis LD, James MN. J Mol Biol. 2007; 366:916. [PubMed: 17196984]
24. Hopkins AL, Groom CR, Alex A. Drug Discov Today. 2004; 9:430. [PubMed: 15109945]
25. Morrison RD, Blobaum AL, Byers FW, Santomango TS, Bridges TM, Stec D, Brewer KA, Sanchez-Ponce R, Corlew MM, Rush R, Felts AS, Manka J, Bates BS, Venable DF, Rodriguez AL, Jones CK, Niswender CM, Conn PJ, Lindsley CW, Emmitte KA, Daniels JS. Drug Metab Dispos. 2012; 40:1834. [PubMed: 22711749]

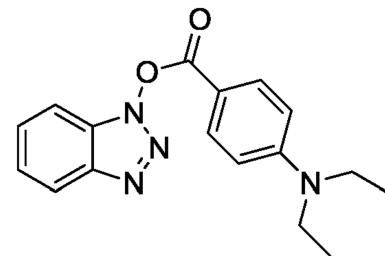
26. For information on MLPCN's probe compound ancillary screen see Eurofins LeadProfilingScreen®: www.eurofinspanlabs.com
27. The protein-ligand X-ray structure of 7-bound SARS-3CLpro has been deposited in PDB. RCSB ID code rcsb081783 and PDB ID code 4MDS



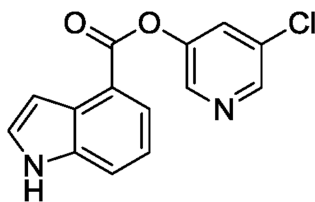
1 (2004)¹⁷
MAC-5576
 $IC_{50} = 0.5 \mu\text{M}$



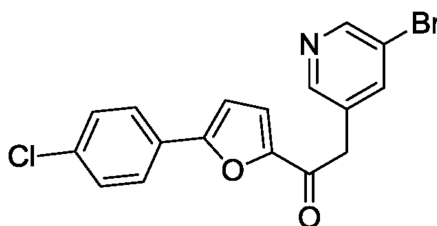
2 (2005)¹⁸
Cinanserin
 $IC_{50} = 5 \mu\text{M}$



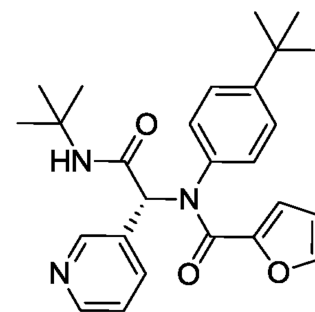
3 (2006)¹⁹
 $K_i = 11.1 \mu\text{M}$



4 (2008)²⁰
 $IC_{50} = 30 \text{ nM}$
SARS-CoV $EC_{50} = 6.9 \mu\text{M}$



5 (2008)²¹
 $IC_{50} = 13 \mu\text{M}$



6, ML188 (2013)²²
 $IC_{50} = 1.5 \mu\text{M}$
SARS-CoV $EC_{50} = 12.9 \mu\text{M}$
pdb code: 3V3M

Figure 1. Representative non-peptidic 3CLpro inhibitors utilizing a warhead and non-covalent mechanism of inhibition (1–6).

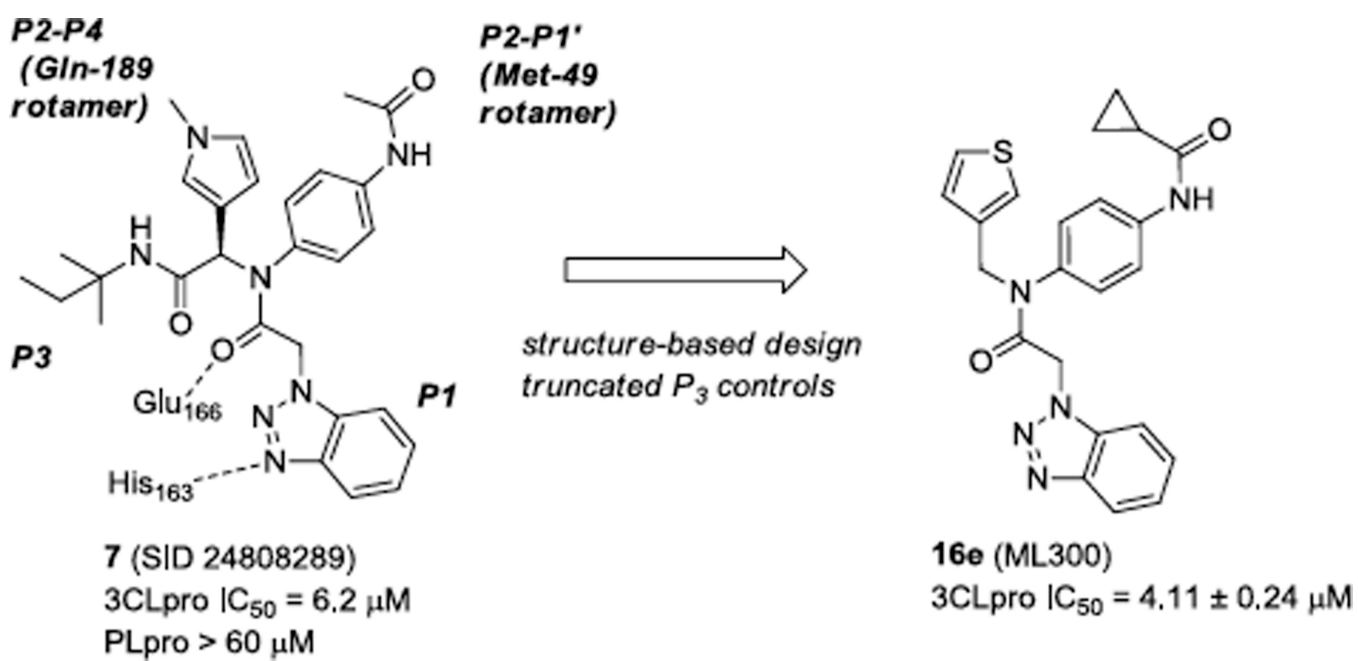


Figure 2.
Binding orientation and properties of MLPCN 3CLpro HTS hit **7** and evolved probe molecule ML300 (**8**).

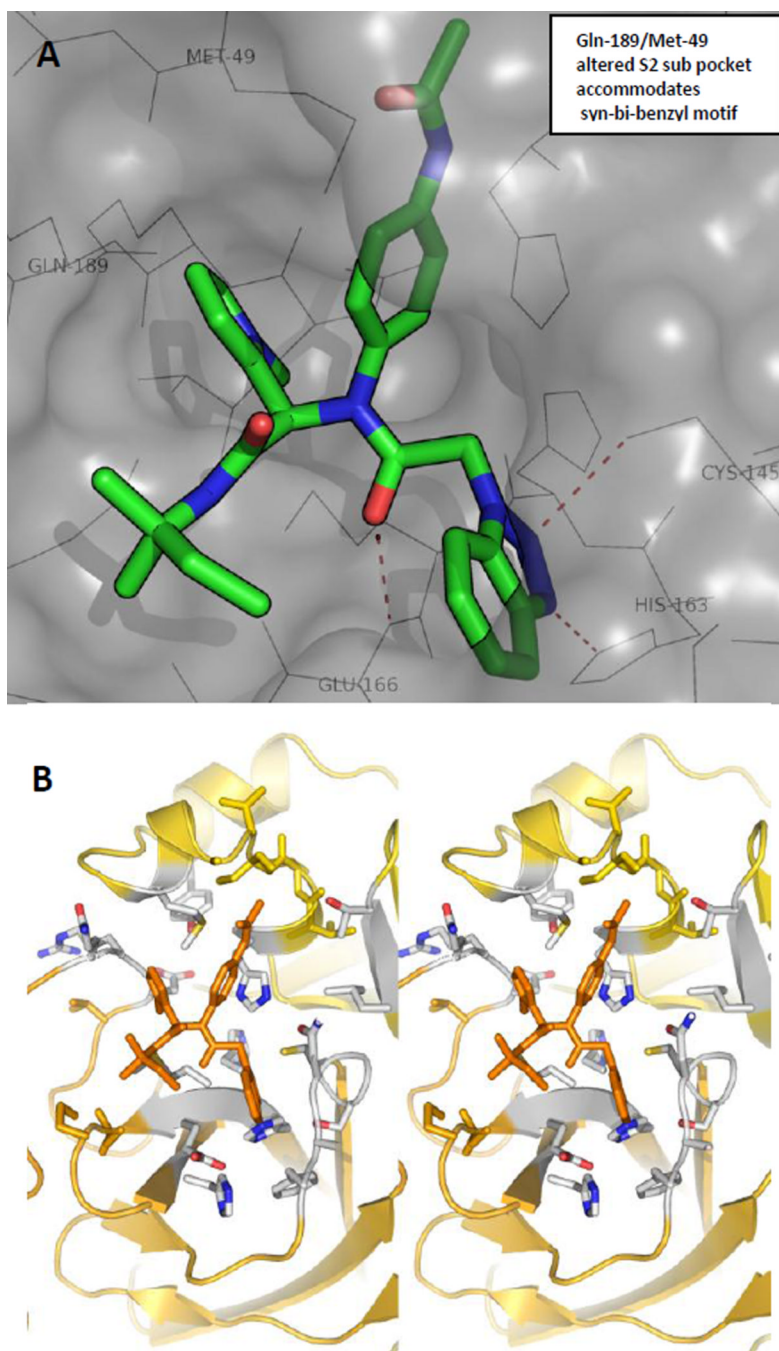
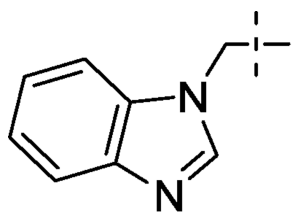
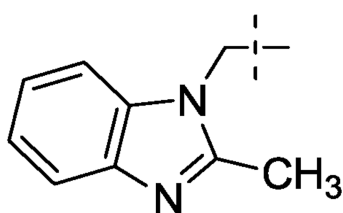


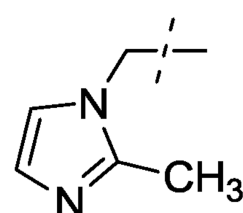
Figure 3.
A) Solvent accessible surface view of 7-3CLpro complex (PDB code: 4MDS, PubChem SID 24808289); B) X-ray crystal structure of 7 (capped sticks in orange carbon) with SARS 3CLpro in wall-eye stereo view with key residues and hydrogen bonds.



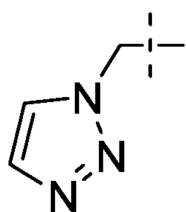
9a
Inactive



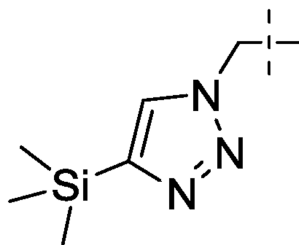
9b
Inactive



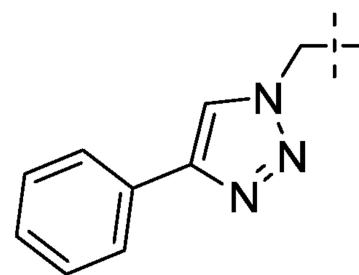
9c
Inactive



10a
Inactive



10b
Inactive



10c
3CLpro IC₅₀ = 11 μM

Figure 4.
Representative azole replacements (**9a–c** and **10a–c**).

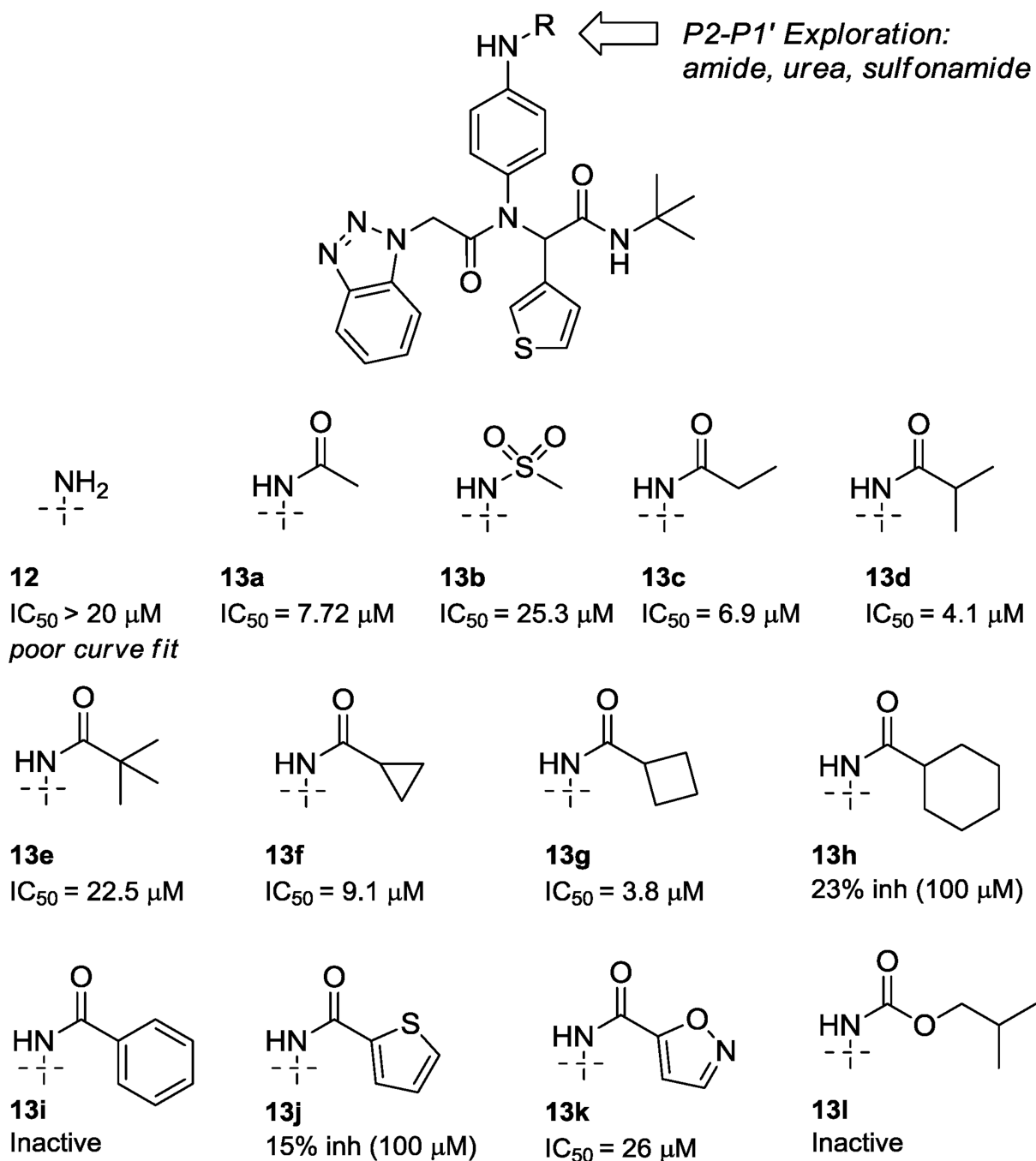
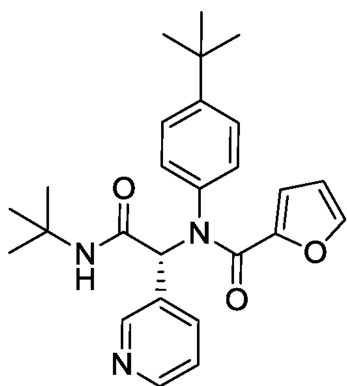


Figure 5.
3CLpro activity from library 13.

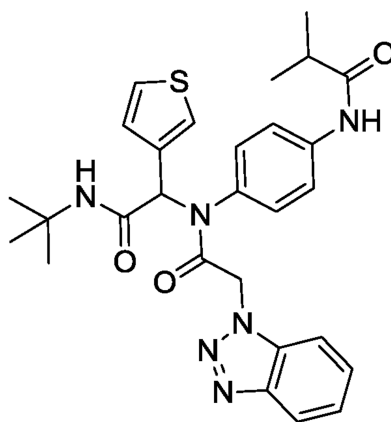
**6 (ML188)**²²

SID 99350510, MW=433

3CLpro IC₅₀ = 1.5 μM

LE=0.25

cLogP=4.6, LELP=18

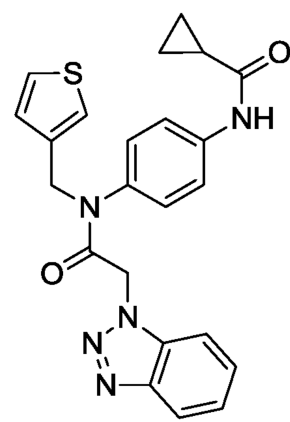
**13d (racemic)**

SID 93373783, MW=532

3CLpro IC₅₀ = 4.1 μM

LE=0.21

cLogP=4.0, LELP=19

**16e (ML300)**

SID 99289112, MW=431

3CLpro IC₅₀ = 4.11 ± 0.24 μM

LE=0.24

cLogP=3.2, LELP=13

In vitro DMPK and ancillary pharmacology:**ML188**

PPB Fu (h, r): 3.3%, 2.6%

CL_{hep} (h, r): 20, 69 mL/min/kg

CYPs (μM):

>30 (1A2), 9.1 (2C9), >30 (2D6), 1.7 (3A4)

Eurofins Profiler Screen:

No significant activity

ML300

PPB Fu (h, r): 4.8%, 10.6%

CL_{hep} (h, r): 20, 67 mL/min/kg

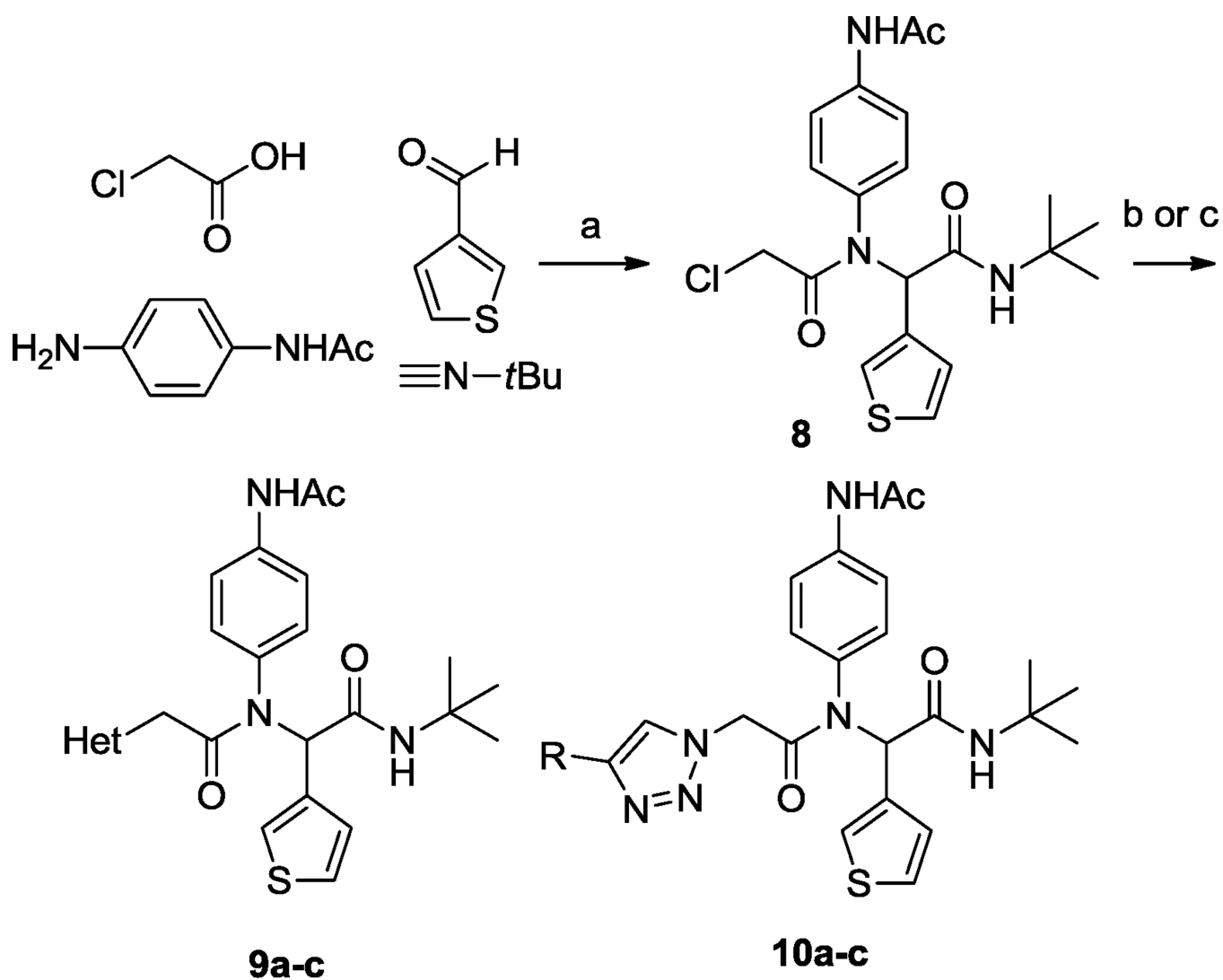
CYPs (μM):

7.7 (1A2), 7.2 (2C9), 8.4 (2D6), 4.6 (3A4)

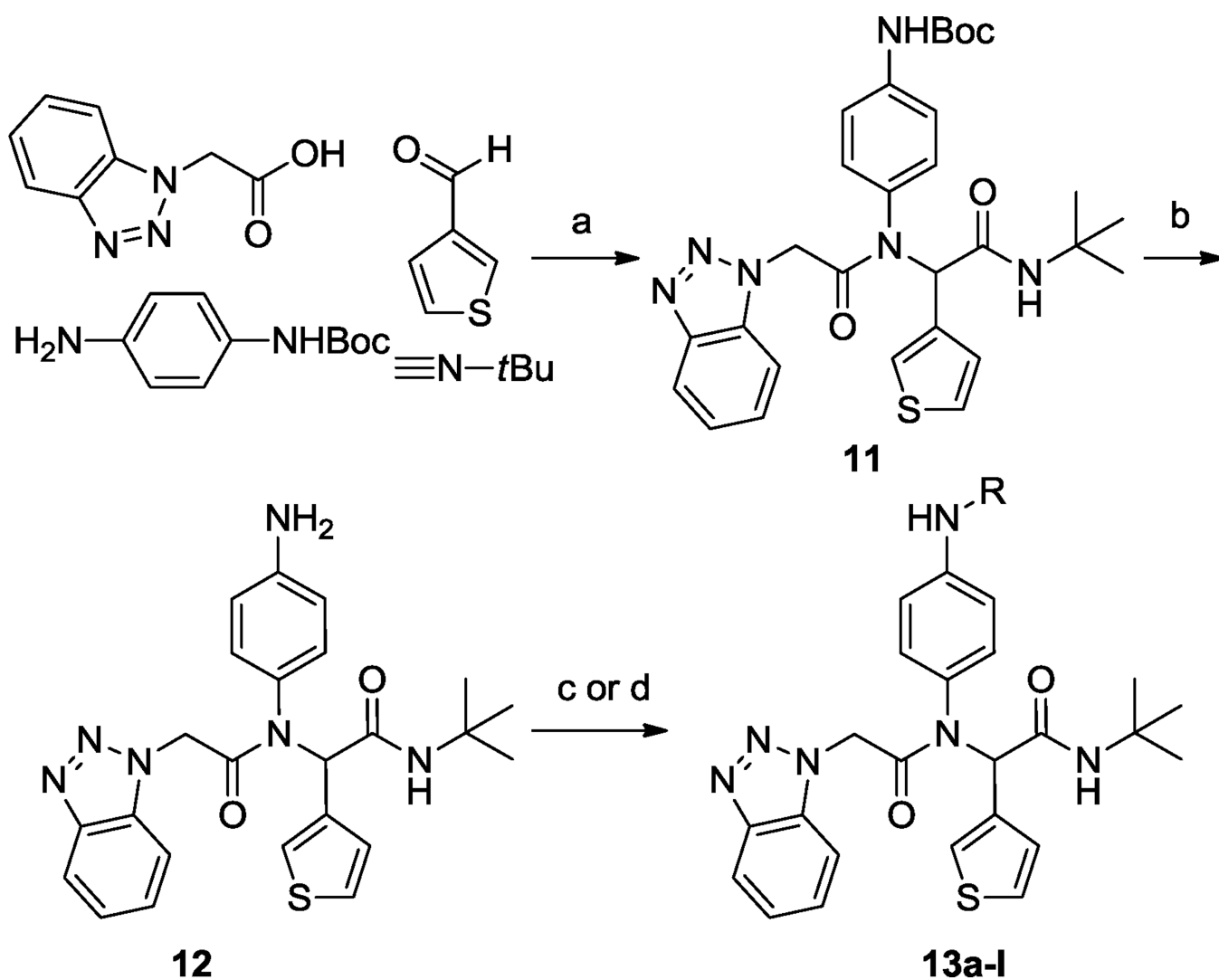
Eurofins Profiler Screen:

Melatonin MT1 75% inhibition (10 μM)

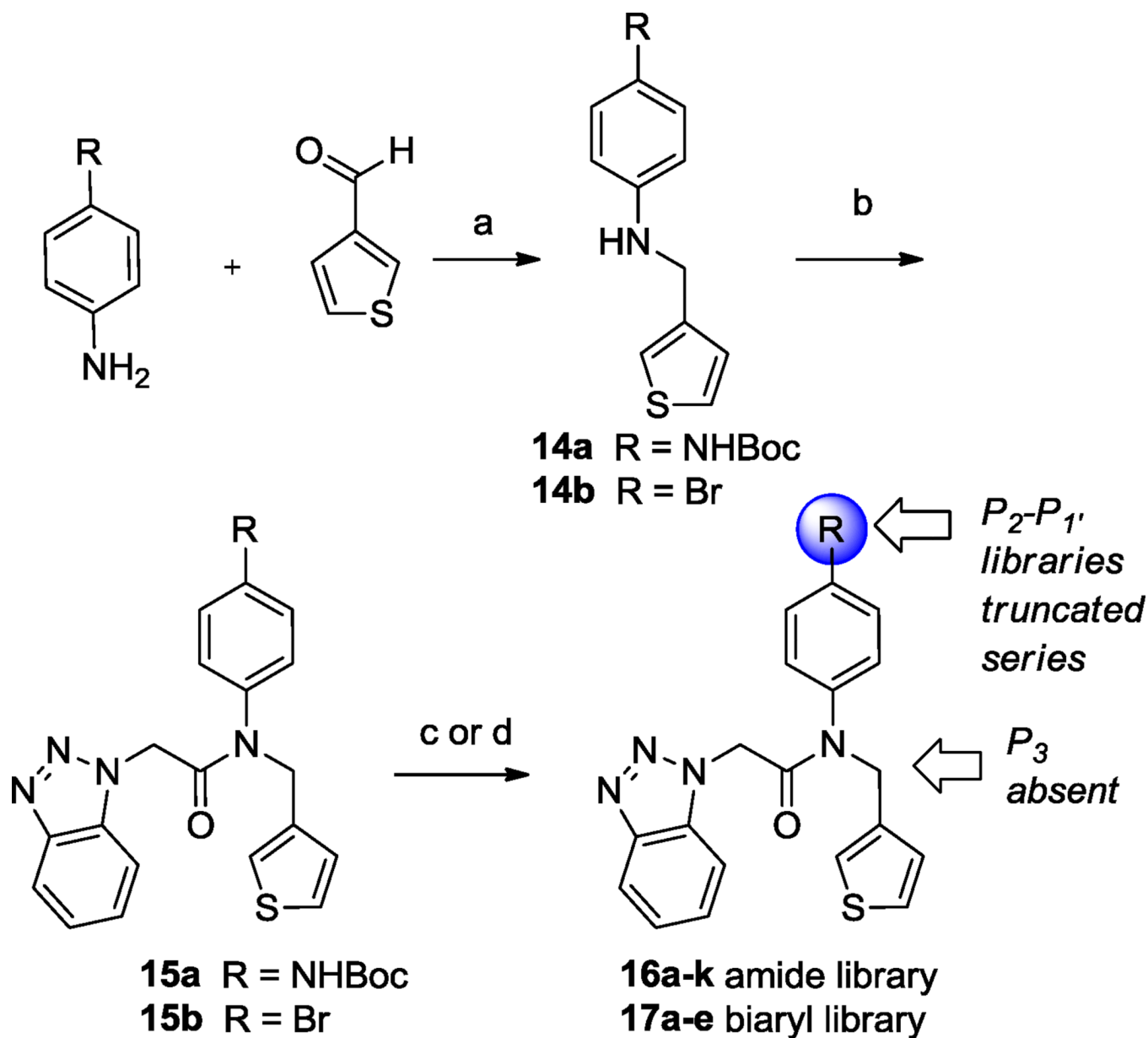
Figure 6.
Profiles of 3CLpro inhibitors **6** (ML188), **13d**, and **16e** (ML300).

**Scheme 1.**

Synthesis of P₁ analogs **9a-c** and **10a-c**. Reagents and conditions: (a) MeOH, 50 °C 4h, 95%, (b) (i) NaH, HetNH, DMF, (ii) **9**, DMF, 65–80%, (c) (i) NaN₃, DMF, 100 °C μwave 30 min., 95%, (ii) acetylene (R=Ph, TMS), DCE, 120 °C 16h, 85–98%, (iii) R = TMS, TBAF, HOAc, 0 °C – rt, 45%. Final library compounds were purified by UV prep or mass-directed prep HPLC.

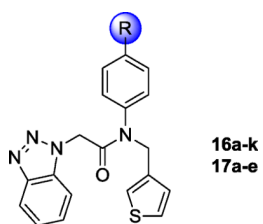
**Scheme 2.**

Synthesis of P₂-P₁ analogs **12** and **13a-l**. Reagents and conditions: (a) MeOH, 50 °C 4h, 94%, (b) TFA, 95% (c) (i) HATU, DIPEA, DMF, RCO₂H, 55–73% (d) RCO₂Cl or RSO₂Cl, TEA, DCM, 51–64%. Final library compounds were purified by UV prep or mass-directed prep HPLC.

**Scheme 3.**

Synthesis of P_2 - P_1 analogs **16a-k** and **17a-e** within truncated series. Reagents and conditions: (a) $\text{NaHB}(\text{OAc})_3$, DCE, rt, 80% (b) benzotriazol-1-yl-acetic acid, HATU, TEA, DMF, rt, 74% (c) (i) **15a**, TFA, DCM, 95%, (ii) HATU, DIPEA, DMF, RCO_2H , 65–80%; RCO_2Cl or RSO_2Cl , TEA, DCM, 90–95%; $\text{NaHB}(\text{OAc})_3$, RCHO, DCE, 45–95% (d) **15b**, Ar/HetB(OH)₂, 1M aq. Na_2CO_3 , 5 mol% $\text{Pd}(\text{PPh}_3)_4$, THF, 30–65%. Final library compounds were purified by UV prep or mass-directed prep HPLC.

Table 1

3CLpro activity **16a–k**, **17a–e**.

Cmpd	R	IC ₅₀ ^a	Cmpd	R	IC ₅₀ ^a
16a		2.9	16i		10.3
16b		3.6	16j		2.1
16c		13.3	16k		1.5
16d		3.4	17a		0.051
16e		4.1	17b		0.97
16f		8.1	17c		0.70
16g		22.1	17d		2.0
16h		18% (100μM)	17e		12.5

^aIC₅₀ are the average of three independent determinations and represent a coefficient of variation (CV) < 0.10